LETTER

doi:10.1038/nature12600

Dendritic spikes enhance stimulus selectivity in cortical neurons *in vivo*

Spencer L. Smith[1,2], Ikuko T. Smith[1,2], Tiago Branco[1,3] & Michael Häusser[1]

Neuronal dendrites are electrically excitable: they can generate regenerative events such as dendritic spikes in response to sufficiently strong synaptic input[1–3]. Although such events have been observed in many neuronal types[4–9], it is not well understood how active dendrites contribute to the tuning of neuronal output *in vivo*. Here we show that dendritic spikes increase the selectivity of neuronal responses to the orientation of a visual stimulus (orientation tuning). We performed direct patch-clamp recordings from the dendrites of pyramidal neurons in the primary visual cortex of lightly anaesthetized and awake mice, during sensory processing. Visual stimulation triggered regenerative local dendritic spikes that were distinct from back-propagating action potentials. These events were orientation tuned and were suppressed by either hyperpolarization of membrane potential or intracellular blockade of NMDA (*N*-methyl-D-aspartate) receptors. Both of these manipulations also decreased the selectivity of subthreshold orientation tuning measured at the soma, thus linking dendritic regenerative events to somatic orientation tuning. Together, our results suggest that dendritic spikes that are triggered by visual input contribute to a fundamental cortical computation: enhancing orientation selectivity in the visual cortex. Thus, dendritic excitability is an essential component of behaviourally relevant computations in neurons.

Neuronal dendrites express voltage-dependent Ca^{2+} and Na^{+} channels that confer electrical excitability, particularly the ability to support the active back-propagation of action potentials and the initiation of local dendritic spikes[1]. In addition, the voltage-dependent Mg^{2+} block of synaptic NMDA receptors can also support nonlinear synaptic integration and dendritic spike initiation[5,10]. These mechanisms of active synaptic integration have been probed extensively *in vitro*[2]. Dendritic spikes have also been observed *in vivo* under certain conditions[6–8]; however, it remains unclear whether they are involved in behaviourally relevant computations[11–13]. To investigate whether dendritic non-linearities can contribute to a well-known example of cortical computation, orientation tuning in the visual cortex[14], we made direct dendritic patch-clamp recordings from layer 2/3 neurons in the mouse visual cortex.

To measure dendritic activity *in vivo*, whole-cell patch-clamp recordings were obtained from the thin apical dendrites (diameter, 2.0 ± 0.4 μm, mean ± s.d.; $n = 12$) of layer 2/3 neurons in the mouse primary visual cortex (Fig. 1a) in lightly anaesthetized and awake mice. The patch-clamp pipette was used to fill cells with a fluorescently labelled Ca^{2+} dye (100 μM Oregon Green 488 BAPTA-1), for imaging Ca^{2+} transients, and a red fluorescent dye (25–50 μM Alexa Fluor 594), for imaging the morphology of the dendritic arbor and identifying the precise location of the dendritic recording (Fig. 1b). Dendritic recordings exhibited the expected physiological features, such as a high local input resistance that increased with distance from the soma[15,16] (Extended Data Fig. 1a–c).

In somatic recordings, visual stimulation with drifting square-wave gratings evoked conventional action potential activity, with the firing rate tuned to the orientation of the stimulus[14,17] (Fig. 1c). By contrast, recordings from distal dendrites (>75 μm from the soma) showed orientation-tuned, high-frequency bursts of Na^{+} spikes riding on a depolarization envelope, a finding that is consistent with the activation of voltage-gated Ca^{2+} channels and synaptic NMDA receptor currents (Fig. 1d–g and Extended Data Fig. 1d). The properties of these spikes were in contrast to those of isolated spikes (single spikes separated by at least 50 ms from other spikes), which are presumed to be back-propagating action potentials (bAPs; Fig. 1d, e), although not all bAPs are isolated bAPs. The isolated bAPs exhibited a uniform amplitude and shape within a recording, and they decreased in amplitude and increased in width with increasing distance from the soma[15] (Extended Data Fig. 1e, f). In contrast to dendritic bursts, which can contain both local Na^{+} spikes and bAPs, isolated bAPs provide a read-out of somatic activity that can be compared with local dendritic events. Visually evoked spike bursts that were recorded in distal dendrites were tuned to the orientation of the stimulus, with reliable trial-to-trial tuning (Fig. 1e, f). The preferred orientation of dendritic spike bursts did not differ from that of bAPs recorded in the same cell (difference in preferred orientation, $34.7 \pm 28.8^{\circ}$; $n = 9$; $P = 0.22$, paired t-test; Extended Data Fig. 2).

We next sought to determine whether these dendritic events were local. Given that dendritic Na^{+} spikes, a prominent feature of the dendritic regenerative events we recorded, have fast kinetics, their waveform is likely to be heavily attenuated by the cable-filtering properties of the dendritic arbor and thus not propagated efficiently to the soma (by contrast, the slow depolarization envelope that typically underlies dendritic regenerative events can spread more readily to the soma[15]). The maximum instantaneous and mean spike rates, as well as the variance-to-mean ratio, were higher in distal dendritic recordings (>75 μm; $n = 9$) than in proximal dendritic recordings (<50 μm; $n = 5$) or somatic recordings (Fig. 2a), suggesting that many of the individual spikes in the bursts observed in distal dendritic recordings are indeed local dendritic spikes and not bAPs[15]. The spike statistics from somatic recordings and proximal dendritic recordings (<50 μm from the soma; 1.7 ± 0.3 μm, mean diameter ± s.d.; $P = 0.14$, two-sample t-test, not different from the diameter of distal dendrites recorded) were indistinguishable ($P > 0.05$, two-sample t-test), thus confirming that the dendritic recording configuration itself does not affect spike rates. These measurements were made in lightly anaesthetized mice, and similar spiking patterns were observed in dendritic recordings from awake mice (Fig. 2a, filled symbols, and Extended Data Fig. 3), demonstrating that such spiking is also present in the alert, behaving animal. These data indicate that, at distal dendritic recording sites, spiking occurs at higher rates and with a higher degree of 'burstiness' than spiking recorded at the soma, and they provide the first piece of evidence that these dendritic events are local.

A second piece of evidence indicating the dendritic origin of these events is provided by the onset, or foot, of the spike waveform. One signature of propagated spikes is a sharp inflection at the foot of the spike, in contrast to the smooth rise observed near the site of spike initiation[18]. Isolated spontaneous spikes exhibited a clear 'kink' at their

[1]Wolfson Institute for Biomedical Research and Department of Neuroscience, Physiology and Pharmacology, University College London, Gower Street, London WC1E 6BT, UK. [2]Department of Cell Biology and Physiology and Neuroscience Center, University of North Carolina School of Medicine, Chapel Hill, North Carolina 27599, USA. [3]Laboratory of Molecular Biology, Medical Research Council, Cambridge CB2 0QH, UK.

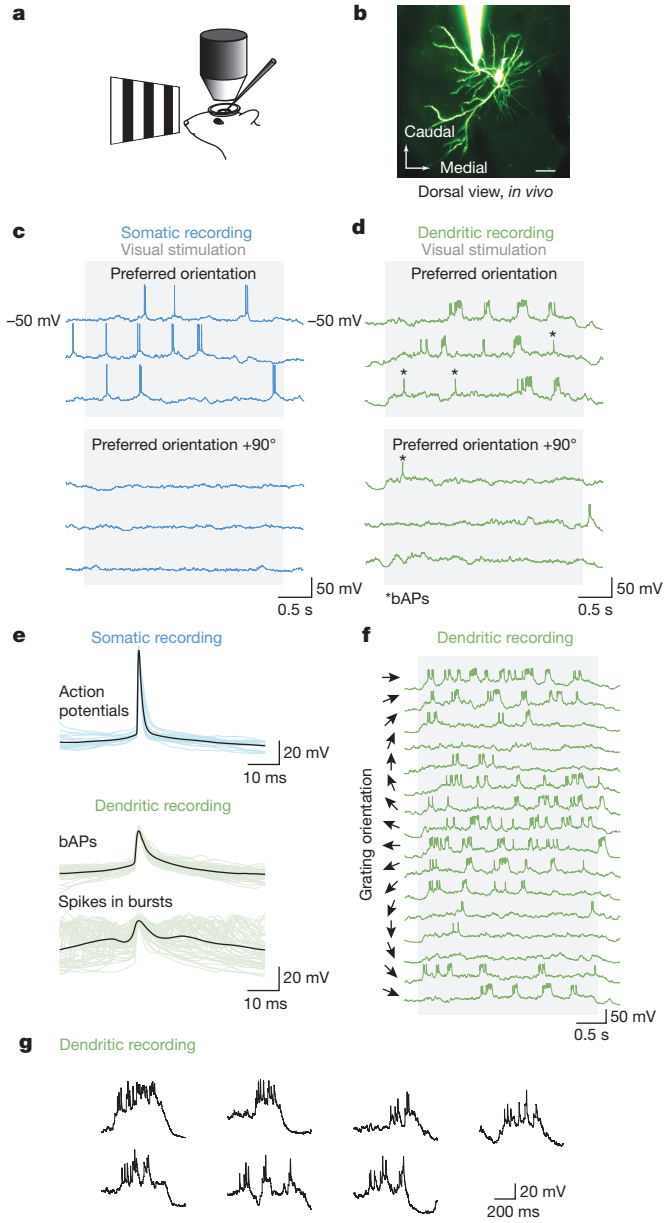

Figure 1 | Dendritic patch-clamp recordings from visual cortex pyramidal neurons *in vivo*. **a**, Schematic of the recording and imaging set-up for *in vivo* dendritic patch-clamp recordings with two-photon microscopy. **b**, A two-photon microscopy image of a layer 2/3 pyramidal neuron in the mouse visual cortex *in vivo*, obtained by filling with Alexa Fluor 594 and dendritic patch-clamp recording at 100 µm from the soma (maximum intensity projection) (scale bar, 20 µm). **c**, **d**, Square-wave grating visual stimuli evoked somatic action potentials (**c**) and dendritic activity (**d**) that exhibited reliable orientation-tuned burst-spiking events. **e**, The spikes within dendritic burst events were highly variable compared with the more stereotyped bAPs and somatically recorded action potentials. **f**, The frequency of dendritic burst events varied with the orientation of the square-wave grating visual stimuli. **g**, Individual burst events were highly variable in amplitude and kinetics (dendritic recording 150 µm from the soma).

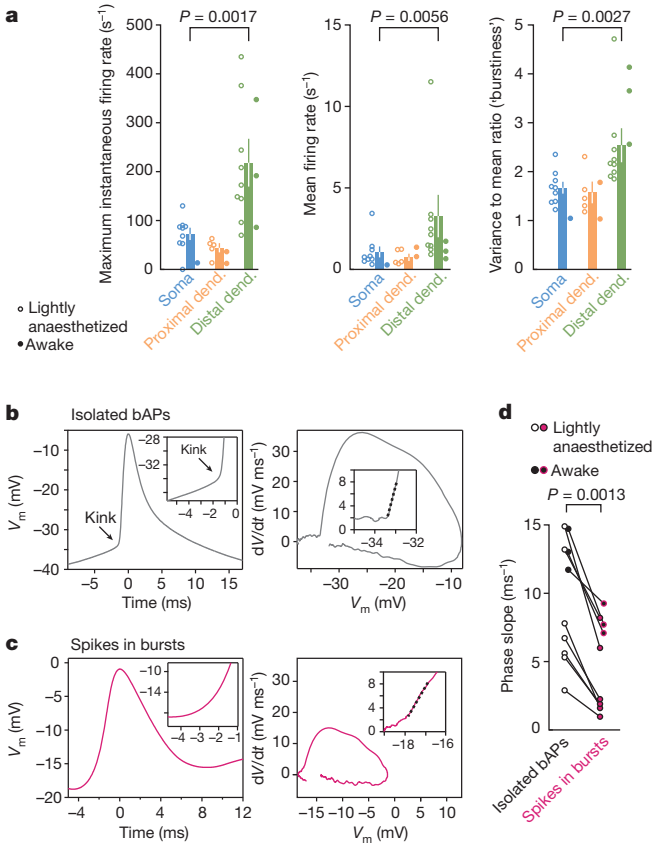

Figure 2 | Visually evoked dendritic burst events are local. **a**, Whole-cell patch-clamp recordings were performed at the soma ($n = 9$), proximal dendritic (proximal dend.) locations (<50 µm from the soma; $n = 5$) or distal dendritic (distal dend.) locations (>75 µm from the soma; $n = 9$). The frequency of stimulus-evoked dendritic burst events at the soma and the proximal dendritic locations were similar; however, the event frequency and burstiness (variance-to-mean ratio of the spike count distribution, or Fano factor) were significantly higher at the distal dendritic locations (P values from the Wilcoxon rank sum test; comparing somatic and distal dendritic recordings). Data from recordings in awake mice ($n = 6$ total) exhibited the same trends as in lightly anaesthetized mice. Error bars indicate s.e.m. **b**, The inflection in membrane potential (V_m) for isolated back-propagated action potentials recorded at distal dendritic locations (>100 µm from the soma) exhibited a sharp kink, consistent with propagated spikes. This is visible both in voltage versus time plots (left) and dV/dt (rate of V_m change, where t is time) versus voltage phase plots (right). The insets show magnifications of the onset at early time points. **c**, By contrast, spikes in bursts exhibited a slower onset, consistent with local generation. **d**, Across the population of dendritic recordings, isolated spikes consistently exhibited sharper inflections at onset (measured as the initial slope in the dV/dt versus voltage phase plots; dashed lines in **b** and **c**) than did spikes in bursts. Distal dendritic recordings from awake mice exhibited the same trend as in lightly anaesthetized mice.

onset, as expected for bAPs (Fig. 2b). Spikes within bursts, by contrast, generally exhibited a much slower onset, indicative of local generation (Fig. 2c). The membrane potential at spike initiation did not completely predict the spike onset speed (Extended Data Fig. 4). Thus, the depolarization envelope during dendritic bursts, which can also reduce the speed of spike onset, did not by itself account for the difference in spike shape. Although these spikes were heterogeneous and were probably a mixed population containing some bAPs, spikes within bursts consistently exhibited a slower onset, across the population, than did isolated bAPs ($P = 0.0013$, Wilcoxon rank sum test; $n = 7$ anaesthetized mice; data from awake mice exhibited the same trend; Fig. 2d), consistent with their identity as locally generated dendritic spikes.

To obtain a third piece of evidence, and a more direct read-out of the relationship between dendritic spikes and somatic action potentials, we used two-photon Ca^{2+} imaging to simultaneously measure Ca^{2+} fluctuations at the soma during dendritic patch-clamp recordings, allowing us to infer somatic action potential activity during dendritic patch-clamp recordings. Spike bursts recorded at distal dendritic sites were correlated with somatic Ca^{2+} signals (Fig. 3a). As was the case with the tuning of dendritic bursts and bAPs, the preferred orientation of dendritic bursts (Fig. 3b) was similar to the preferred orientation of the somatic Ca^{2+} signal (Fig. 3c), with qualitative differences in the

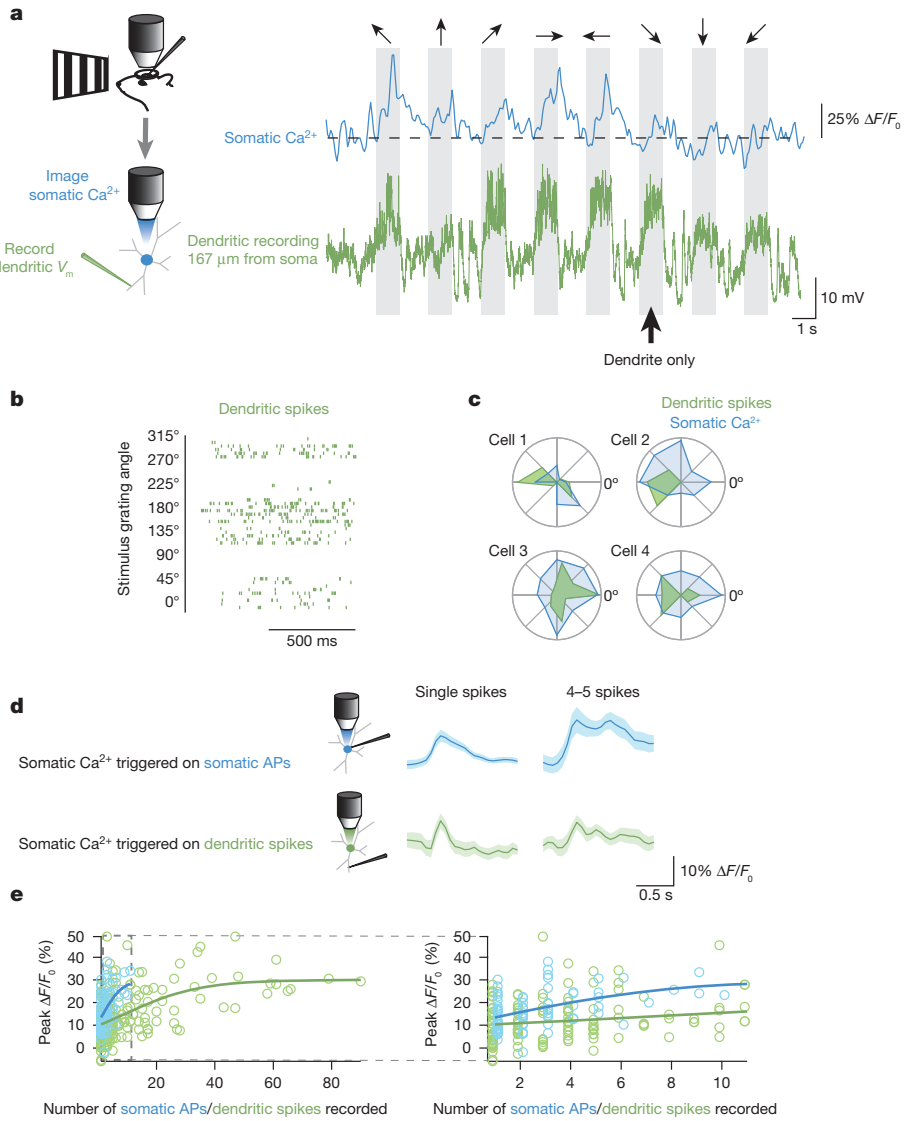

Figure 3 | Simultaneous dendritic recording and Ca^{2+} imaging at the soma shows that dendritic spikes are local. **a**, To infer spiking activity at the soma during dendritic patch-clamp recordings, neurons were filled with a Ca^{2+} indicator and somatic Ca^{2+} signals were imaged. During simultaneous dendritic voltage recordings and somatic Ca^{2+} imaging, dendritic bursts were sometimes not accompanied by robust somatic Ca^{2+} signals (indicated with a heavy arrow). Arrows at the top indicate the orientation of the visual stimulus grating, with shaded boxes indicating the duration of stimulus presentation. **b**, **c**, Dendritic bursting was well tuned (**b**) and overlapped with the orientation tuning at the soma (**c**). (The data for Cell 1 are shown in **a** and **b**.) **d**, To calibrate the Ca^{2+} signals seen at the soma, we calculated spike-triggered averages of the somatic Ca^{2+} signal for well-isolated single spikes and bouts of four to five spikes (within 640 ms). The somatic Ca^{2+} signal amplitude was similar for single spikes regardless of whether the spikes were recorded at the soma or the dendrite. No difference in Ca^{2+} signal amplitude was found between bouts of four to five spikes recorded at the dendrite and single spikes recorded at the soma, suggesting that some dendritic spikes were local. **e**, Across the population of events, even though the Ca^{2+} signals became saturated at about the same magnitude (fluorescence change over baseline $\Delta F/F_0 \sim 30\%$; not different between the two configurations, $P = 0.99$, two-sample t-test), the somatic Ca^{2+} signal as a function of the number of dendritic spikes rose much more slowly than that for the somatically recorded spikes (left). Data from responses with fewer than ten spikes are presented magnified (right).

tuning curves consistent with the interpretation that a single dendrite contributes only a portion of the input that drives a neuron to fire. To calibrate these measurements, we used separate somatic recordings combined with somatic Ca^{2+} imaging. The somatic Ca^{2+} signal observed during a dendritic burst of four to five spikes was indistinguishable from the Ca^{2+} signal observed during a single action potential recorded at the soma ($P = 0.77$, two-sample t-test; Fig. 3d). Furthermore, although the somatic Ca^{2+} signals became saturated near the same level in both dendritic and somatic recording configurations (fluorescence change over baseline $\Delta F/F_0 \sim 30\%$ for both configurations; not different between the two configurations, $P = 0.99$, two-sample t-test), this saturation level was reached with only 10 spikes recorded at the soma but needed more than 40 spikes in the dendrite ($P < 10^{-8}$, the two distributions are different, multivariate Kolmogorov–Smirnov test; $n = 5$; Fig. 3e). Thus, many of the individual spikes in bursts recorded at the dendrite were probably locally generated, rather than each reflecting a bAP, and resulted in subthreshold depolarizations at the soma. Measurements of Ca^{2+} signals at the site of distal dendritic recordings (Extended Data Fig. 5a) provided further evidence that individual dendritic spikes were locally generated, by showing that dendritic bursts with Ca^{2+} signals spanning all of the visible dendritic branches (Extended Data Fig. 5b) contained spikes with steeper onsets than did bursts with Ca^{2+} transients that were confined to the local recording site and not observed in adjacent branches[19] ($n = 78$ dendritic bursts; Extended Data Fig. 5c–f). Together, these results demonstrate how dendritic spikes, local Ca^{2+} signals and bAPs interact during visual processing.

A final piece of evidence that dendritic bursts consist of locally generated dendritic spikes is that visually evoked dendritic bursts were

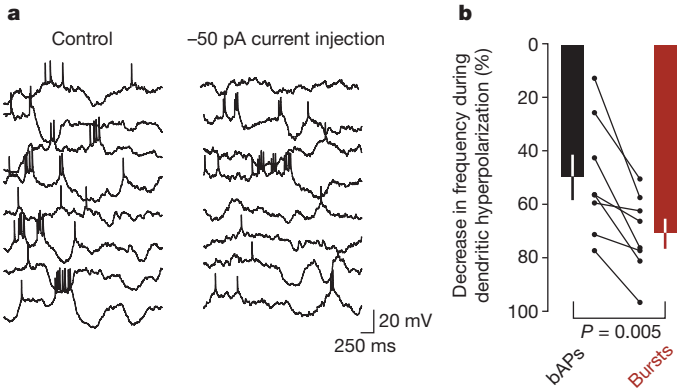

Figure 4 | Hyperpolarization decreases the frequency of dendritic bursts. **a**, An example dendritic recording shows that compared to control conditions (left), hyperpolarization (right) decreased the mean frequency of bursts (from 0.32 Hz to 0.14 Hz; −68%) more than the mean frequency of bAPs (0.51 Hz to 0.36 Hz; −30%). **b**, Population data showing that bursts and bAPs were both suppressed ($P = 3.0 \times 10^{-6}$ and $P = 0.0004$, respectively, *t*-test) and that bursts were suppressed to a greater degree by hyperpolarization than were bAPs ($P = 0.005$, paired *t*-test). Bars indicate population means and error bars indicate s.e.m. for the decrease in mean rates of bAPs and dendritic bursts during hyperpolarization compared with the control condition. Data from individual dendritic recordings are shown between the two bars, with lines connecting data points from the same recording.

more sensitive to local dendritic hyperpolarization than were bAPs. When a steady hyperpolarizing current was delivered through the dendritic patch-clamp pipette, the rate of burst events decreased more than did the rate of isolated bAPs ($P = 0.005$, paired *t*-test; Fig. 4), indicating that the dendritic burst-generating mechanisms were more sensitive to the local membrane potential than were the mechanisms that support back-propagation of somatic action potentials. Taken together, these findings indicate that the spike bursts recorded at the dendrite during visual processing are not a pure population of bAPs but rather consist mainly of locally generated dendritic spikes.

We next sought to uncover how dendritic regenerative events evoked by visual stimulation might influence the orientation tuning of neuronal output. The prolonged depolarization envelope of dendritic bursts can propagate to the soma and influence axonal output. If dendritic bursts, and the somatic depolarizations they cause, are required for normal synaptic integration during visual processing, then blocking them might disrupt an important cortical computation: orientation tuning. Layer 2/3 neurons exhibited spiking that was robustly orientation tuned[17], as well as subthreshold responses (Fig. 5a–d; even when the cells fired few to no spikes, Extended Data Fig. 6). The subthreshold tuning closely matched the spike-based tuning in terms of preferred orientation[20] (Pearson's correlation coefficient $R = 0.83$, $P < 10^{-5}$; Extended Data Fig. 7a) and orientation selectivity (as measured by the membrane potential orientation selectivity index, V_mOSI; Pearson's $R = 0.88$, $P = 0.0040$; Extended Data Fig. 7b). This subthreshold tuning provides a way to compare synaptic integration in the control condition and the hyperpolarized condition where dendritic spikes are prevented (Fig. 4). Hyperpolarization degraded this subthreshold orientation tuning both in terms of the modulation amplitude (Fig. 5e, f) and the V_mOSI (Fig. 5g), without changing the preferred orientation (Pearson's $R = 0.88$, $P = 0.022$; $n = 10$; Extended Data Fig. 7c, d). This effect was not accounted for by changes in the driving force for Cl^- ions (Pearson's $R = 0.34$, $P = 0.15$; Extended Data Fig. 8). These results demonstrate that voltage-gated mechanisms are required for normal synaptic integration and subthreshold orientation tuning during visual processing, which is consistent with the hypothesis that dendritic regenerative events enhance subthreshold orientation tuning.

The synaptic NMDA receptor current, which is subject to voltage-dependent Mg^{2+} block, is a prime candidate for linking synaptic input

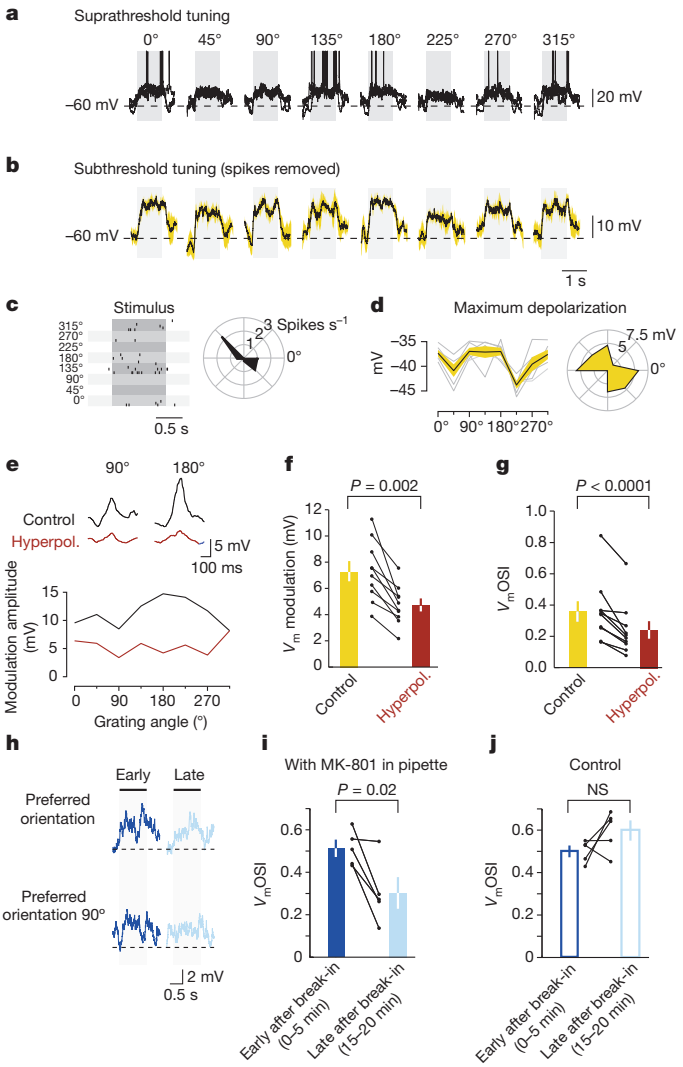

Figure 5 | Dendritic mechanisms contribute to the selectivity of subthreshold orientation tuning. **a**, **b**, Somatic whole-cell recording from a layer 2/3 pyramidal neuron, exhibiting robust visually evoked spiking (three sweeps overlaid; stimulus duration indicated by the grey bars) (**a**) and subthreshold responses (50-ms windows around the spikes were blanked, and the same results were obtained when the blanking window was decreased to 20 ms) (**b**). **c**, **d**, The responses in **a** and **b** were orientation tuned as indicated by spike rasters (**c**) and polar plots of maximal depolarization (**d**). **e**–**g**, Hyperpolarization (hyperpol.) decreased the amplitude of the stimulus-evoked membrane potential modulation and decreased its tuning selectivity (**e**): it decreased V_m modulation amplitude (**f**) and decreased the V_m orientation selectivity index (OSI) (**g**) across the population. **h**–**j**, To investigate the mechanisms involved in the dendritic spikes contributing to orientation tuning, whole-cell somatic patch-clamp recordings were performed with 1 μM MK-801 in the pipette solution. **h**, The orientation tuning selectivity progressively decreased during the recording as MK-801 diffused into the cell and blocked NMDA channels. In these example traces, the response to the preferred orientation decreased from early in the recording to late in the recording. **i**, Across the population, subthreshold orientation tuning was strongly inhibited at late time points in the recording compared with early time points. **j**, In control recordings, with no blockers in the pipette solution, the orientation tuning selectivity did not significantly change across the recording and was not significantly different from the early period of MK-801 recordings ($P > 0.05$, two-sample *t*-test). Bars in **f**–**i** and **j** represent population means, and error bars indicate s.e.m. Between the bars, the individual data points are shown, and lines connect data taken in the same recording.

to regenerative events in dendrites[10,15]. Visually driven synaptic input to layer 2/3 pyramidal cells activates synaptic NMDA receptors[21]. To determine whether NMDA receptors form one of the voltage-dependent

mechanisms that contributes to nonlinear synaptic integration *in vivo*, we used whole-cell somatic recordings with a use-dependent, intracellular NMDA receptor blocker, MK-801, included in the pipette solution[22]. Intracellular MK-801 did not affect up and down state dynamics (Extended Data Fig. 9a, b), confirming that the manipulation was restricted to the recorded cell, and dendritic spiking in the recorded cell was blocked by MK-801 (Extended Data Fig. 9c, d). Early in these recordings, before effective NMDA receptor block, the subthreshold orientation tuning was normal; however, late in these recordings, after MK-801 had diffused through the dendritic tree, V_mOSI decreased markedly (Fig. 5h–j), as did spike-based tuning (OSI early in recording, 0.82 ± 0.12; late in recording, 0.45 ± 0.17; $P = 0.016$, paired t-test; $n = 5$; Fig. 5i, j). Because the orientation selectivity was degraded despite the remaining, unblocked, receptor pathways (for example, AMPA (α-amino-3-hydroxy-5-methyl-4-isoxazole propionic acid) receptors and metabotropic glutamate receptors), we conclude that NMDA receptor currents are crucial for the tuning of synaptic integration in these neurons and that their depolarization-dependent relief from Mg^{2+} block might be a key mechanism that links synaptic input and dendritic regenerative events, including dendritic spikes[5,10].

We have presented multiple lines of evidence, including direct dendritic recordings, showing that visually evoked sensory input triggers local dendritic spikes in cortical pyramidal neurons *in vivo*. Moreover, we have shown that hyperpolarization decreases both the rate of dendritic spiking and V_mOSI, thus demonstrating that voltage-dependent dendritic mechanisms help shape the input–output function of neurons during sensory processing[23]. Finally, we have also provided evidence for at least one specific biophysical mechanism that could underlie these dendritic events: NMDA receptor current. Together, these results show that the synaptic integration of sensory input crucially relies on voltage-dependent dendritic mechanisms.

A detailed compartmental model of layer 2/3 pyramidal cells confirmed that a biophysically plausible model can account for our data (Supplementary Note 1, Extended Data Fig. 10 and Supplementary Videos 1–3). This model reproduced the key findings of this study and offers potential mechanistic insight. For example, passively propagated Na^+ spikes can arrive immediately after an actively generated spike on a dendrite and support instantaneous spike rates of several hundred Hertz, as observed in distal dendritic recordings (Fig. 2a). In addition, cooperative recruitment of NMDA receptor current provides a crucial link between synaptic input and fast dendritic spiking. These results show that basic biophysical mechanisms support the electrophysiological phenomena that we observed in direct dendritic recordings *in vivo*.

Our experimental results and compartmental modelling suggest that synaptic input causes a dendritic depolarization that activates voltage-dependent ion channels and relieves the Mg^{2+} block of NMDA receptors[5,10,15]. This results in a supralinear, local regenerative event that includes dendritic Na^+ spikes. The slow time course of the NMDA receptor current component of the regenerative events causes a prolonged depolarization envelope that propagates to the soma and enhances axonal output. Thus, local computational subunits generated by voltage-dependent mechanisms in dendrites[22,24] are activated by sensory input *in vivo*, provide an orientation-tuned signal to the soma and thereby help determine stimulus selectivity.

Dendritic regenerative events provide a mechanism by which a relatively small number of inputs can drive spike output[24,25], changing the effective connectivity between local functional groups of neurons[26] or mitigating the noise in cortical circuits[27], by ensuring that variable synaptic input can result in a more reliable postsynaptic response. Our data from experiments on awake mice demonstrate that these dendritic events occur during alert sensory processing[28]. Because dendrite-targeting inhibitory interneurons are inhibited in awake mice during sensory stimulation[29], this circuitry might have a key role in gating sensory input[30]. Overall, our results demonstrate that dendrites are not passive integrators of sensory-driven input *in vivo*. Rather, sensory input engages dendritic voltage-dependent mechanisms and thereby generates local regenerative events and dendritic spikes, which have an important role in shaping orientation selectivity, a quintessential cortical computation.

METHODS SUMMARY

Wild-type C57BL/6 mice (24–56 days old, both male and female) were anaesthetized with isoflurane (5% for induction, 1.5–2.5% for surgery and 0–0.5% during recording), augmented with chlorprothixene (0.5–2 mg kg^{-1}). Experiments with awake mice were carried out with head fixation, during which mice could freely move their limbs, groom and drink a sweet liquid reward when offered. Square-wave gratings (0.04 cycles per degree, 2 cycles s^{-1}) were displayed on a liquid crystal display (LCD) screen to map orientation selectivity. The screen was shrouded with a cone up to the eye of the mouse to prevent contamination of the imaging pathway with light from the visual stimulus. For both dendritic and somatic recordings, the pipette solution contained 135 mM or 140 mM K^+ methylsulphate, 4 mM or 10 mM KCl, 10 mM HEPES, 10 mM Na_2-phosphocreatine, 4 mM Mg-ATP, 0.3 mM Na_2-GTP, 0.1 mM Oregon Green 488 BAPTA-1 and 0.025–0.050 mM Alexa Fluor 594; pH adjusted with KOH to 7.2; 290 mmol kg^{-1}. Pipette resistances ranged from 4.9 MΩ to 11 MΩ (mean, 7.9 MΩ) for dendritic recordings and from 5 MΩ to 8 MΩ (mean, 6.9 MΩ) for somatic recordings. All recordings were from the apical dendrites of superficial layer 2/3 pyramidal neurons. Unlike layer 5 neurons or deeper layer 2/3 neurons, these neurons do not have a prominent apical trunk and tuft; therefore, the recorded dendrites were geometrically similar to basal dendrites. A custom-built two-photon microscope with a 16× magnification and 0.8 numerical aperture water immersion objective (Nikon) and a large aperture collection pathway was used to visualize neurons. In dendritic recordings, putative bAPs were automatically identified as single spikes when isolated from other spikes by at least 50 ms. Unless otherwise specified, all measurements are expressed as mean ± s.e.m.

Online Content Any additional Methods, Extended Data display items and Source Data are available in the online version of the paper; references unique to these sections appear only in the online paper.

Received 16 August 2012; accepted 22 August 2013.

Published online 27 October; corrected online 6 November 2013 (see full-text HTML version for details).

1. Johnston, D. & Narayanan, R. Active dendrites: colorful wings of the mysterious butterflies. *Trends Neurosci.* **31,** 309–316 (2008).
2. London, M. & Häusser, M. Dendritic computation. *Annu. Rev. Neurosci.* **28,** 503–532 (2005).
3. Spruston, N. Pyramidal neurons: dendritic structure and synaptic integration. *Nature Rev. Neurosci.* **9,** 206–221 (2008).
4. Larkum, M. E., Zhu, J. J. & Sakmann, B. A new cellular mechanism for coupling inputs arriving at different cortical layers. *Nature* **398,** 338–341 (1999).
5. Schiller, J., Major, G., Koester, H. J. & Schiller, Y. NMDA spikes in basal dendrites of cortical pyramidal neurons. *Nature* **404,** 285–289 (2000).
6. Helmchen, F., Svoboda, K., Denk, W. & Tank, D. W. *In vivo* dendritic calcium dynamics in deep-layer cortical pyramidal neurons. *Nature Neurosci.* **2,** 989–996 (1999).
7. Llinas, R., Nicholson, C., Freeman, J. A. & Hillman, D. E. Dendritic spikes and their inhibition in alligator Purkinje cells. *Science* **160,** 1132–1135 (1968).
8. Kamondi, A., Acsady, L. & Buzsaki, G. Dendritic spikes are enhanced by cooperative network activity in the intact hippocampus. *J. Neurosci.* **18,** 3919–3928 (1998).
9. Yuste, R., Gutnick, M. J., Saar, D., Delaney, K. R. & Tank, D. W. Ca^{2+} accumulations in dendrites of neocortical pyramidal neurons: an apical band and evidence for two functional compartments. *Neuron* **13,** 23–43 (1994).
10. Branco, T., Clark, B. A. & Häusser, M. Dendritic discrimination of temporal input sequences in cortical neurons. *Science* **329,** 1671–1675 (2010).
11. Ferster, D. & Jagadeesh, B. EPSP-IPSP interactions in cat visual cortex studied with *in vivo* whole-cell patch recording. *J. Neurosci.* **12,** 1262–1274 (1992).
12. Volgushev, M., Pei, X., Vidyasagar, T. R. & Creutzfeldt, O. D. Postsynaptic potentials in cat visual cortex: dependence on polarization. *Neuroreport* **3,** 679–682 (1992).
13. Hirsch, J. A., Alonso, J. M. & Reid, R. C. Visually evoked calcium action potentials in cat striate cortex. *Nature* **378,** 612–616 (1995).
14. Hubel, D. H. & Wiesel, T. N. Receptive fields of single neurones in the cat's striate cortex. *J. Physiol. (Lond.)* **148,** 574–591 (1959).
15. Larkum, M. E., Waters, J., Sakmann, B. & Helmchen, F. Dendritic spikes in apical dendrites of neocortical layer 2/3 pyramidal neurons. *J. Neurosci.* **27,** 8999–9008 (2007).
16. Waters, J. & Helmchen, F. Background synaptic activity is sparse in neocortex. *J. Neurosci.* **26,** 8267–8277 (2006).
17. Niell, C. M. & Stryker, M. P. Highly selective receptive fields in mouse visual cortex. *J. Neurosci.* **28,** 7520–7536 (2008).
18. Yu, Y., Shu, Y. & McCormick, D. A. Cortical action potential backpropagation explains spike threshold variability and rapid-onset kinetics. *J. Neurosci.* **28,** 7260–7272 (2008).

19. Svoboda, K., Helmchen, F., Denk, W. & Tank, D. W. Spread of dendritic excitation in layer 2/3 pyramidal neurons in rat barrel cortex *in vivo*. *Nature Neurosci.* **2,** 65–73 (1999).
20. Tan, A. Y., Brown, B. D., Scholl, B., Mohanty, D. & Priebe, N. J. Orientation selectivity of synaptic input to neurons in mouse and cat primary visual cortex. *J. Neurosci.* **31,** 12339–12350 (2011).
21. Jia, H., Rochefort, N. L., Chen, X. & Konnerth, A. Dendritic organization of sensory input to cortical neurons *in vivo*. *Nature* **464,** 1307–1312 (2010).
22. Polsky, A., Mel, B. W. & Schiller, J. Computational subunits in thin dendrites of pyramidal cells. *Nature Neurosci.* **7,** 621–627 (2004).
23. Lavzin, M., Rapoport, S., Polsky, A., Garion, L. & Schiller, J. Nonlinear dendritic processing determines angular tuning of barrel cortex neurons *in vivo*. *Nature* **490,** 397–401 (2012).
24. Mel, B. W. Synaptic integration in an excitable dendritic tree. *J. Neurophysiol.* **70,** 1086–1101 (1993).
25. Smith, S. L. & Häusser, M. Parallel processing of visual space by neighboring neurons in mouse visual cortex. *Nature Neurosci.* **13,** 1144–1149 (2010).
26. Ohiorhenuan, I. E. *et al.* Sparse coding and high-order correlations in fine-scale cortical networks. *Nature* **466,** 617–621 (2010).
27. London, M., Roth, A., Beeren, L., Häusser, M. & Latham, P. E. Sensitivity to perturbations *in vivo* implies high noise and suggests rate coding in cortex. *Nature* **466,** 123–127 (2010).
28. Xu, N. L. *et al.* Nonlinear dendritic integration of sensory and motor input during an active sensing task. *Nature* **492,** 247–251 (2012).
29. Gentet, L. J. *et al.* Unique functional properties of somatostatin-expressing GABAergic neurons in mouse barrel cortex. *Nature Neurosci.* **15,** 607–612 (2012).
30. Jiang, X., Wang, G., Lee, A. J., Stornetta, R. L. & Zhu, J. J. The organization of two new cortical interneuronal circuits. *Nature Neurosci.* **16,** 210–218 (2013).

Supplementary Information is available in the online version of the paper.

Acknowledgements We are grateful to B. Clark, P. Latham, M. London, D. Ringach, A. Roth, C. Schmidt-Hieber and C. Wilms for discussions and comments on the manuscript. This work was supported by the following: a Long-Term Fellowship and a Career Development Award from the Human Frontier Science Program and a Klingenstein Fellowship (S.L.S.); a Helen Lyng White Fellowship (I.T.S.); a Wellcome Trust and Royal Society Fellowship and MRC Programme Leader Track (T.B.); and by grants from the Wellcome Trust, ERC and Gatsby Charitable Foundation (M.H.).

Author Contributions S.L.S. and M.H. conceived and designed the experiments. S.L.S. and I.T.S. performed the experiments. S.L.S. analysed the data. T.B. designed and carried out the compartmental modelling. S.L.S., I.T.S., T.B. and M.H. interpreted the data and wrote the paper.

Author Information Reprints and permissions information is available at www.nature.com/reprints. The authors declare no competing financial interests. Readers are welcome to comment on the online version of the paper. Correspondence and requests for materials should be addressed to S.L.S. (slab@unc.edu) or M.H. (m.hausser@ucl.ac.uk).

METHODS

Preparation. All experiments were carried out in accordance with the regulations of the UK Home Office or the guidelines and regulations of the US Department of Health and Human Services and the University of North Carolina. Wild-type C57BL/6 mice (24–56 days old, male and female) were anaesthetized with isoflurane (5% for induction, 1.5–2.5% for surgery and 0–0.5% during recording), augmented with chlorprothixene (0.5–2 mg kg^{-1}). During recording, this regime resulted in a sedated state in which the animals did not voluntarily move but responded to a toe pinch. Increased levels of isoflurane (>0.5%) typically suppressed spiking activity, including dendritic bursts. Experiments with awake mice were carried out with head fixation, during which mice could routinely move their limbs, groom and drink a sweet liquid reward when offered.

After gluing a head plate to the skull for head fixation during surgery and recording, a 2–3-mm diameter craniotomy was performed over the monocular visual cortex. A thin layer of agar (1.5%) was dissolved in artificial cerebrospinal fluid (150 mM NaCl, 2.5 mM KCl, 10 mM HEPES, 2 mM $CaCl_2$ and 1 mM $MgCl_2$; pH adjusted with NaOH to 7.3; 300 mmol kg^{-1}) and placed on top of the brain to help dampen movement. A homeothermic heat pad was used to maintain the body temperature within the physiological range, and a water-based ophthalmic ointment was used to maintain eye health.

Visual stimulation. Visual stimulus presentation was controlled by routines written in MATLAB (MathWorks) using the Psychophysics Toolbox extensions[31,32]. Square-wave gratings (0.04 cycles per degree, 2 cycles s^{-1}) of black (2 cd m^{-2}) and white (86 cd m^{-2}) bars in eight different orientations were displayed on a liquid crystal display (LCD) screen (ESAW 7-inch VGA and composite TFT monitor, set at 1024 × 768 resolution and a 60 Hz refresh rate) to map orientation selectivity. The screen was shrouded with a cone up to the eye of the mouse to prevent contamination of the imaging pathway with light from the visual stimulus. The visual stimulus extended from +20° to +124° in azimuth and from −10° to +42° in elevation. Visual stimuli were presented in a shuffled order: each orientation was presented once per sweep of eight orientations, and the order of the orientations was different in each sweep.

Patch-clamp recordings. For both dendritic and somatic recordings, the pipette solution contained 135 mM or 140 mM K^+ methylsulphate, 4 mM or 10 mM KCl, 10 mM HEPES, 10 mM Na_2-phosphocreatine, 4 mM Mg-ATP, 0.3 mM Na_2-GTP, 0.1 mM Oregon Green 488 BAPTA-1 and 0.025–0.050 mM Alexa Fluor 594; pH adjusted with KOH to 7.2; 290 mmol kg^{-1}. Pipette resistances ranged from 4.9 MΩ to 11 MΩ (mean, 7.9 MΩ) for dendritic recordings and from 5 MΩ to 8 MΩ (mean, 6.9 MΩ) for somatic recordings. For dendritic recordings, imaging[33] was used to guide the pipette away from blood vessels and somata, and tip resistance measured using a voltage step in voltage-clamp mode was used to detect contact with a dendrite. Shadowpatching techniques[33] were used to directly target the pipette to the soma. In somatic hyperpolarization experiments, cells were hyperpolarized by 21.4 ± 11.4 mV (mean ± s.d.; from a membrane potential of −49.4 ± 6.7 mV to −70.8 ± 9.4 mV, mean ± s.d.; average V_m across all stimuli after removing spikes). All dendritic recordings were from the apical dendrites of superficial layer 2/3 pyramidal neurons. These neurons do not have a large apical trunk and tuft, unlike layer 5 or deeper layer 2/3 neurons ; therefore, the recorded dendrites were geometrically similar to basal dendrites. The series resistance was 39 ± 5 MΩ and 34 ± 5 MΩ for dendritic and somatic recordings, respectively. The series resistance did not change as a function of dendritic distance from the soma (Pearson's $R = -0.24$, linear regression, $P = 0.50$; $n = 13$). The bridge was rebalanced as needed during the recording. R_{series} increased less than 2% over the time it took to run a tuning curve. In one case, we obtained two distal dendritic recordings in the same mouse. In all other cases, we obtained at most one distal dendritic recording per mouse.

Compartmental modelling. Simulations were performed with the NEURON simulation environment (version 7.2) using a detailed reconstruction of a biocytin-filled layer 2 pyramidal neuron (NeuroMorpho.org ID Martin, NMO_00904). Passive parameters were $C_m = 1\ \mu F\ cm^{-2}$, $R_m = 7{,}000\ \Omega\ cm^2$, $R_i = 100\ \Omega$ cm, yielding a somatic input resistance of 110 MΩ, similar to the experimentally measured mean value (Extended Data Fig. 1a). AMPA, NMDA and $GABA_A$ (γ-aminobutyric acid A) synapses had a peak conductance of 1 nS and were modelled as a bi-exponential function, with time constants of AMPA $\tau 1 = 0.1$ ms, AMPA $\tau 2 = 1$ ms, NMDA $\tau 1 = 2$ ms, NMDA $\tau 2 = 20$ ms, $GABA_A\ \tau 1 = 0.1$ ms and $GABA_A\ \tau = 4$ ms (the inhibition reversal potential was set to −80 mV). The Mg^{2+} block of NMDA synapses was modelled according to Jahr and Stevens[34]. Active conductances were introduced in the soma and in all dendritic compartments and included the following: voltage-activated Na^+ channels (soma 100 mS cm^{-2} and dendrite 60 mS cm^{-2}, distributed as a hot spot in the centre of each branch)[35]; high-voltage activated Ca^{2+} channels (soma 0.05 mS cm^{-2} and dendrite 0.05 mS cm^{-2}); low-voltage activated Ca^{2+} channels (soma 0.3×10^{-3} mS cm^{-2} and dendrite 0.15×10^{-3} mS cm^{-2}); voltage-activated K^+ channels (10 mS cm^{-2} soma and 0.3 mS cm^{-2} dendrite); M-type K^+ channels (soma 0.22 mS cm^{-2} and dendrite 0.1 mS cm^{-2}); and Ca^{2+}-activated K^+ channels (soma 0.3 mS cm^{-2} and dendrite 0.3 mS cm^{-2}). The time course of dendritic Ca^{2+} was modelled by adding the current carried by voltage-activated Ca^{2+} channels and the calcium fraction of the NMDA current (10%)[36] and convolving it with a decaying exponential with a 50 ms time constant. AMPA and NMDA components were colocalized and coactivated at each excitatory synapse.

A total of 1,100 synapses were randomly distributed across the dendritic tree: 80% excitatory and 20% inhibitory. The synapses were separated into background and signal synapses (the signal synapses constituted 10% of the total synapse number) and were activated with independent Poisson spike trains delivered to each synapse. The background synapses were continuously activated at a mean rate of 0.5 Hz, and the signal synaptic input was activated at 5–8 Hz after a 200 ms baseline and stayed active for 200 ms. The results did not depend on the total number of synapses but rather the total input rate. For example, 100 synapses activated at 1 Hz yielded the same result as 1,000 synapses activated at 0.1 Hz (the model did not include short-term plasticity).

Imaging. A custom-built two-photon microscope using galvanometer-based scan mirrors (6-mm diameter, Cambridge Technologies) with a 16× magnification, 0.8 numerical aperture water immersion objective (Nikon) and a large aperture collection pathway with low-noise photomultiplier tubes (models 3896 and 7422-40P, Hamamatsu) was used to image neurons. Frame scans (15.6 frames s^{-1}) and line scans (1 ms per line) were acquired using ScanImage[37].

Analysis. Custom programs written for MATLAB and IGOR Pro (WaveMetrics), including event detection and analysis routines in IGOR Pro by T. Ishikawa (Jikei University), were used for analysis. Input resistance was measured as the steady-state membrane potential in response to a current step. Maximum instantaneous firing rates were computed as the reciprocal of the smallest interspike interval. In dendritic recordings, putative bAPs were automatically identified as single spikes when isolated from other spikes by at least 50 ms.

Statistics. Unless otherwise specified, all measurements are expressed as mean ± s.e.m. The Shapiro–Wilk test was used, before the application of two-sided parametric tests, to confirm that the deviation of the data from normality was statistically insignificant. For non-normal data, or data with significantly different variances, non-parametric tests were used as noted in the text (for example, the Wilcoxon rank sum test used in Fig. 2). The multivariate Kolmogorov–Smirnov test was computed using the generalization of Fasano and Franceschini[38]. Experimental manipulations (hyperpolarization and MK-801 block of NMDA receptors) did not involve randomization or blinding because each recorded cell served as its own control (control versus hyperpolarized or early versus late recording, respectively). Sample sizes were designed to reliably measure neurophysiological parameters while remaining in compliance with ethical guidelines to minimize the number of animals used. The results from Fig. 2a remain statistically significant ($P < 0.05$) when the top one or two data points from the distal dendritic recordings are omitted from the analysis. To test the statistical significance of the orientation tuning of dendritic bursts, we first computed the OSI of the measured dendritic burst firing. We then shuffled the responses so that their associated orientation was assigned at random. We then computed the OSI of the new, reshuffled, responses. This procedure was repeated 1,000 times. The P value was taken as the fraction of time for which a randomly shuffled response yielded an OSI equal to or greater than the actual response.

Orientation tuning analysis. The OSI was computed after fitting a sum of two Gaussian curves to the orientation tuning curve (whether based on spiking or membrane potential), with the centres 180° apart:

$$\mathrm{OSI} = \frac{R_p - R_o}{R_p + R_o}$$

where R_p is the response to the preferred orientation and R_o is the response at the orthogonal orientation. Cells in which the sum of squared residuals between the Gaussian fit and the observed data was less than 15% of the maximum value of the Gaussian fit were considered to be well described by the Gaussian fit.

Membrane potential (V_m) modulation in response to visual stimuli was computed by taking the peak-to-trough amplitude of the cycle average at 2 Hz (the drift rate of the visual stimulus gratings) (after removing any spikes). This modulation can be seen in the traces in Fig. 5c, particularly at 135° and 315°.

31. Brainard, D. H. The psychophysics toolbox. *Spat. Vis.* **10,** 433–436 (1997).
32. Pelli, D. G. The VideoToolbox software for visual psychophysics: transforming numbers into movies. *Spat. Vis.* **10,** 437–442 (1997).
33. Kitamura, K., Judkewitz, B., Kano, M., Denk, W. & Häusser, M. Targeted patch-clamp recordings and single-cell electroporation of unlabeled neurons *in vivo*. *Nature Methods* **5,** 61–67 (2008).
34. Jahr, C. E. & Stevens, C. F. Voltage dependence of NMDA-activated macroscopic conductances predicted by single-channel kinetics. *J. Neurosci.* **10,** 3178–3182 (1990).

35. Nevian, T., Larkum, M. E., Polsky, A. & Schiller, J. Properties of basal dendrites of layer 5 pyramidal neurons: a direct patch-clamp recording study. *Nature Neurosci.* **10,** 206–214 (2007).
36. Spruston, N., Jonas, P. & Sakmann, B. Dendritic glutamate receptor channels in rat hippocampal CA3 and CA1 pyramidal neurons. *J. Physiol. (Lond.)* **482,** 325–352 (1995).
37. Pologruto, T. A., Sabatini, B. L. & Svoboda, K. ScanImage: flexible software for operating laser scanning microscopes. *Biomed. Eng. Online* **2,** 13 (2003).
38. Fasano, G. & Franceschini, A. A multidimensional version of the Kolomogorov–Smirnov test. *Mon. Not. R. Astron. Soc.* **225,** 155–170 (1987).

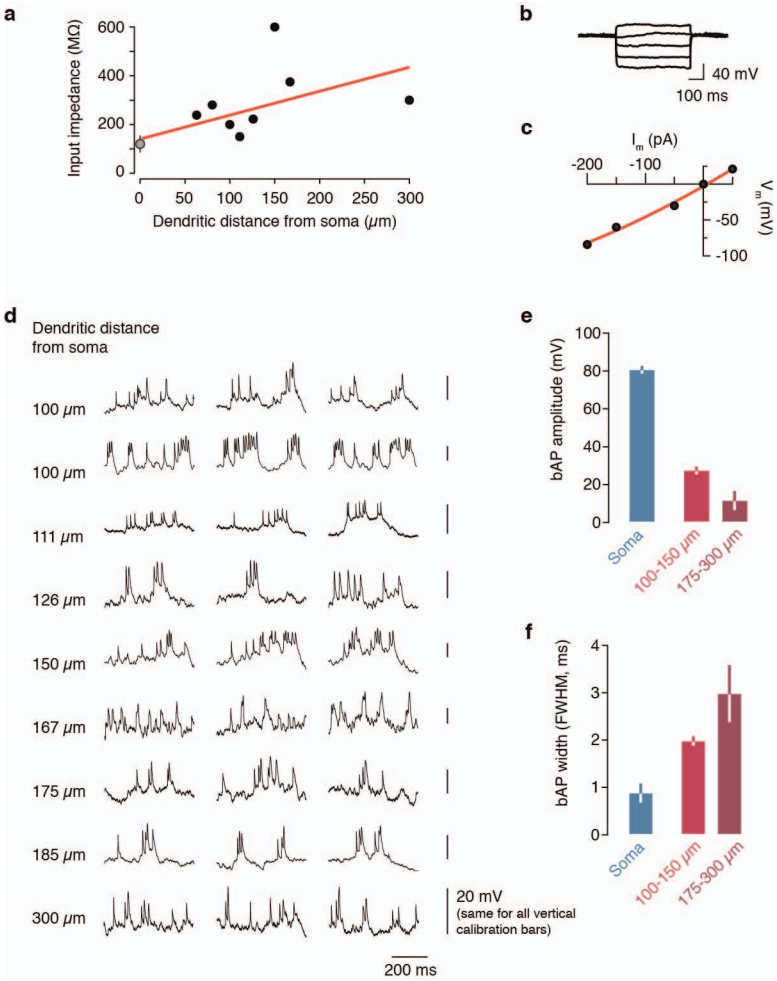

Extended Data Figure 1 | Electrophysiological features of layer 2/3 dendrites *in vivo*. **a**, The input resistance of distal dendrites was typically 100–300 MΩ but sometimes larger (up to 600 MΩ). The input resistance increased as function of dendritic distance from the soma, approximately doubling every 300 μm. The grey point indicates the input resistance measured in somatic patch-clamp recordings (mean ± s.e.m.). **b**, During a dendritic recording at 150 μm from the soma, hyperpolarizing current steps did not reveal a voltage sag; thus, there is probably little to no hyperpolarization-activated cation current, I_h, in the dendrites of layer 2/3 pyramidal neurons *in vivo*. **c**, The peak voltage response plotted against the hyperpolarizing current step amplitude in an I–V plot was well fit by a linear function, confirming the lack of I_h. **d**, Representative dendritic bursts evoked by visual stimulation at the optimal orientation in nine different dendritic recordings at progressively increasing distances from the soma. All right-hand scale bars are 20 mV. **e**, **f**, Compared with action potentials recorded at the soma, bAPs had a lower amplitude (**e**) and were prolonged in time (**f**), and both of these trends were more pronounced with increasing dendritic distance from the soma (error bars, s.d.). Both the amplitude and width were significantly different among the three groups ($P < 0.01$, unpaired t-tests with the Bonferroni correction for multiple comparisons).

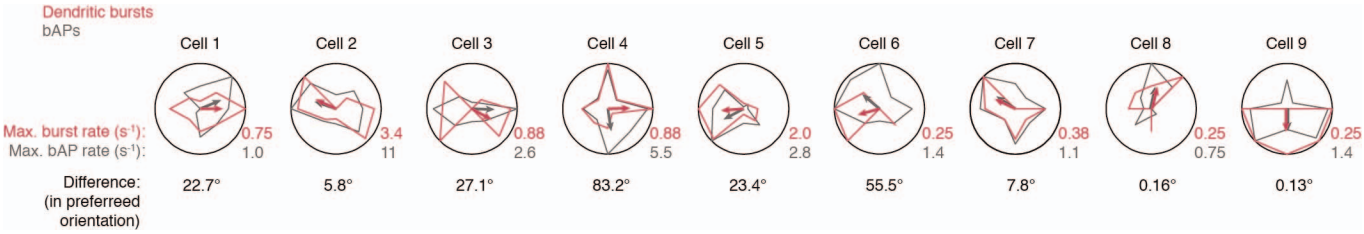

Extended Data Figure 2 | Orientation tuning curves of dendritic bursts compared with bAPs. Tuning curves for dendritic spike bursts and bAPs recorded at distal dendritic locations (>75 μm from soma) are shown. The tuning curves for dendritic bursts match the tuning curves for isolated bAPs. The statistical significance of dendritic burst tuning curves was tested by randomly shuffling responses (details in the Methods) and was found to be significant ($P < 0.05$) for 7 out of 9 cells (dendritic burst tuning in cells 6 and 9 was not significant). The curves were normalized to the maximal values, which are shown at the bottom right of each polar plot. The small qualitative differences may be due to dendrites that are topologically distant from the dendritic recording site exhibiting slightly different tuning curves. The grating drift direction that elicited the largest response is indicated with an arrow. The difference between these directions is indicated at the bottom of each polar plot. The cross correlation between dendritic bursts and isolated bAPs was highly significant: Pearson's $R = 0.54$, $P = 0.000013$, paired t-test; $n = 9$. When only the spikes in the bursts with rise times in the slowest quartile of the distribution were considered to be dendritic in origin, the preferred orientation of bAPs and the slowest quartile were still matched within individual dendritic recordings (difference in preferred orientation, $41.5 \pm 58.1^{\circ}$; $P = 0.49$, paired t-test; $n = 9$).

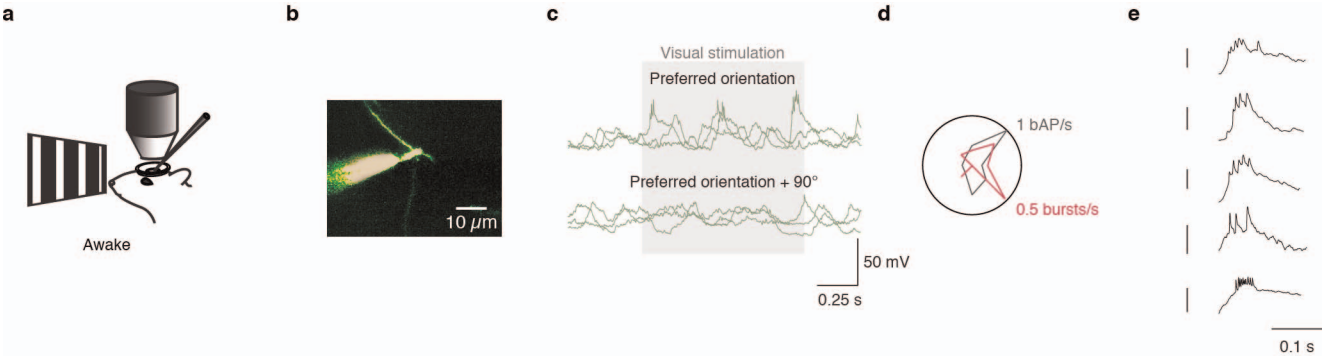

Extended Data Figure 3 | Dendritic recordings in awake mice exhibit dendritic bursts. **a**, Awake, head-fixed mice viewed drifting gratings during electrophysiological recordings. **b**, A two-photon image of the patched dendrite (117 μm from the soma) of a layer 2/3 pyramidal neuron in the mouse visual cortex, after filling with Alexa Fluor 594 with the dendritic patch-clamp pipette. **c**, Dendritic bursts were observed when the preferred orientation was presented. **d**, Tuning curves for the isolated bAPs and dendritic bursts. **e**, Example bursts from three different distal dendritic recordings in awake mice. Calibration bars, 25 mV.

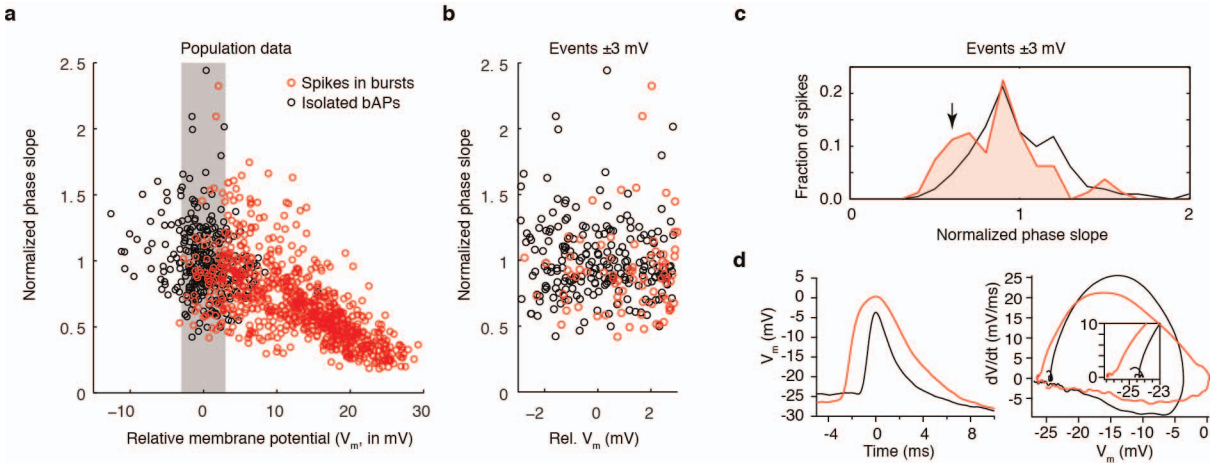

Extended Data Figure 4 | The diversity of onset dynamics versus membrane potential. **a**, Spikes from each distal dendritic recording (both isolated bAPs (black) and spikes in dendritic burst events (red)) were normalized such that isolated bAPs had a mean phase slope of 1. The mean baseline membrane potential (V_m) of isolated bAPs was subtracted from the mean baseline V_m of all spikes. Although many spikes in bursts had a depolarized baseline V_m relative to isolated spikes, there was overlap between the two populations around ±3 mV. **b**, Magnification of panel **a** to show spikes at ±3 mV relative to the mean baseline V_m of isolated bAPs. **c**, Histograms of the two populations reveal a tendency towards lower phase slope values for spikes in bursts ($P = 0.041$, Kolmogorov–Smirnov test ; $n = 211$ bAPs, 80 spikes in bursts). **d**, An example of bAPs and a spike in a burst (both from the same distal dendritic recording): although the bAP has a more depolarized baseline V_m, it still exhibits a steeper phase slope (a kink at the foot of the voltage waveform), indicative of a propagated action potential.

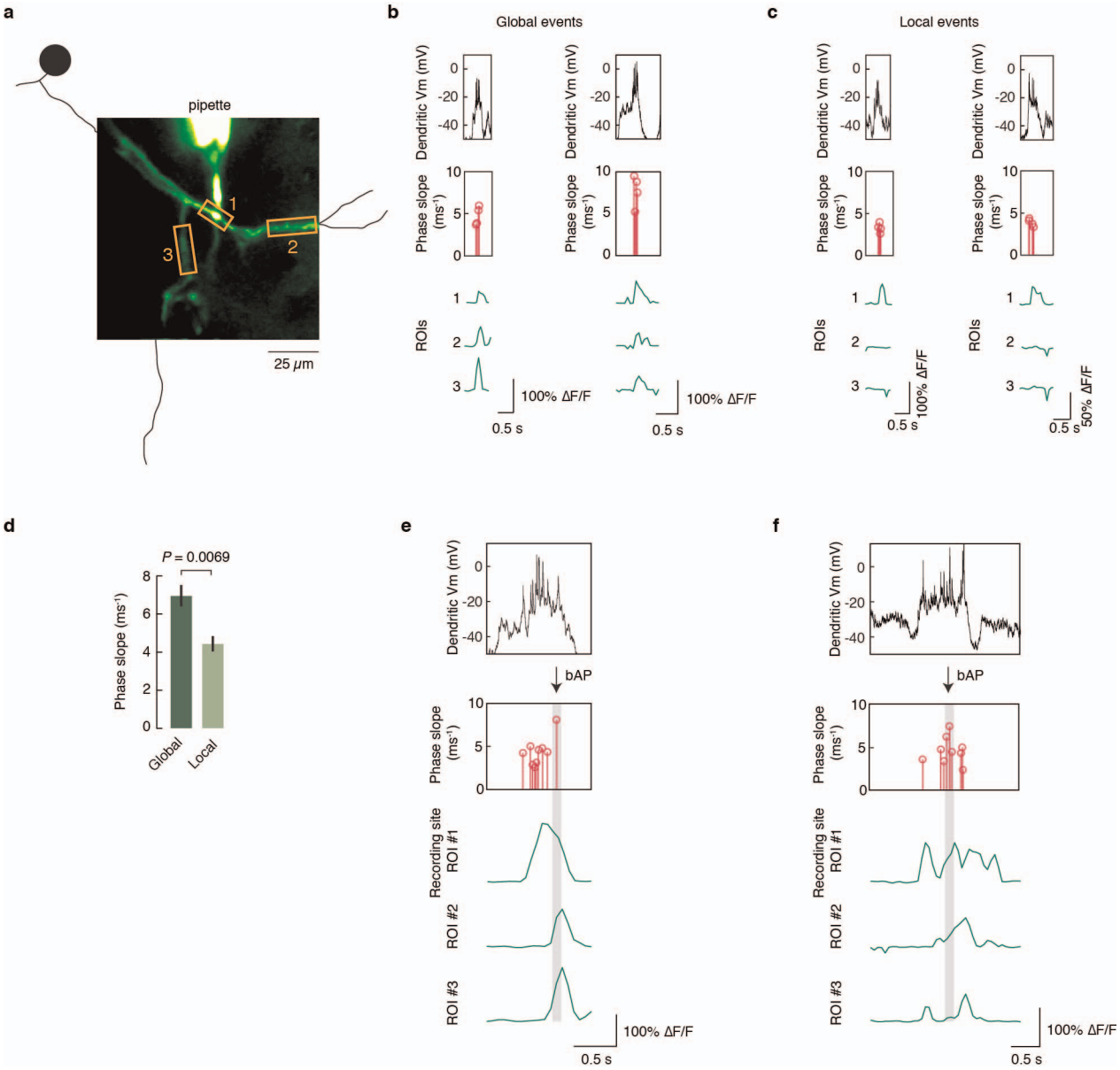

Extended Data Figure 5 | Ca^{2+} imaging at the site of dendritic recording reveals that global Ca^{2+} signals are associated with faster onset spikes. **a**, During dendritic recordings, Ca^{2+} signals were simultaneously imaged at the site of the recording and at nearby dendrites. **b**, In dendritic bursts with global Ca^{2+} signals that were simultaneously observed in all regions of interest (ROIs), the spikes recorded at the dendrite exhibited steep onsets, indicating that they were probably bAPs. **c**, In local Ca^{2+} signals that were observed only in the ROI at the site of recording, the dendritic spikes exhibited slower onsets, indicating that they were probably locally generated. **d**, The maximum phase slope of spikes occurring during global Ca^{2+} events was higher than for spikes occurring during local Ca^{2+} events ($P = 0.0069$, t-test). **e**, **f**, When global Ca^{2+} signals occurred during ongoing local Ca^{2+} signals, the initiation was associated with a steep onset spike. Two examples are shown.

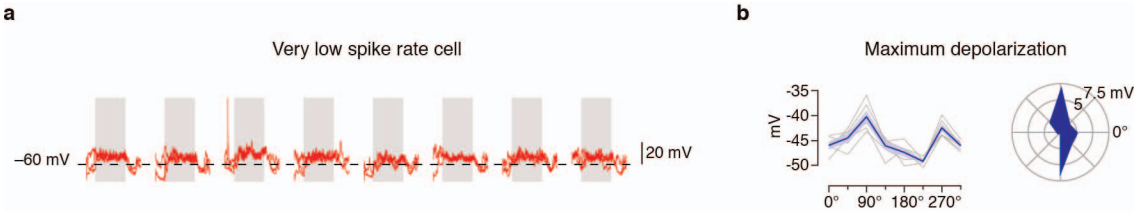

Extended Data Figure 6 | Non-firing cells exhibit subthreshold orientation tuning. **a**, Raw data for an example cell in which subthreshold orientation tuning was observed, although no spikes were fired during stimulus presentations. **b**, In this case, the tuning width of the subthreshold membrane potential was quite sharp and was confined to two directions.

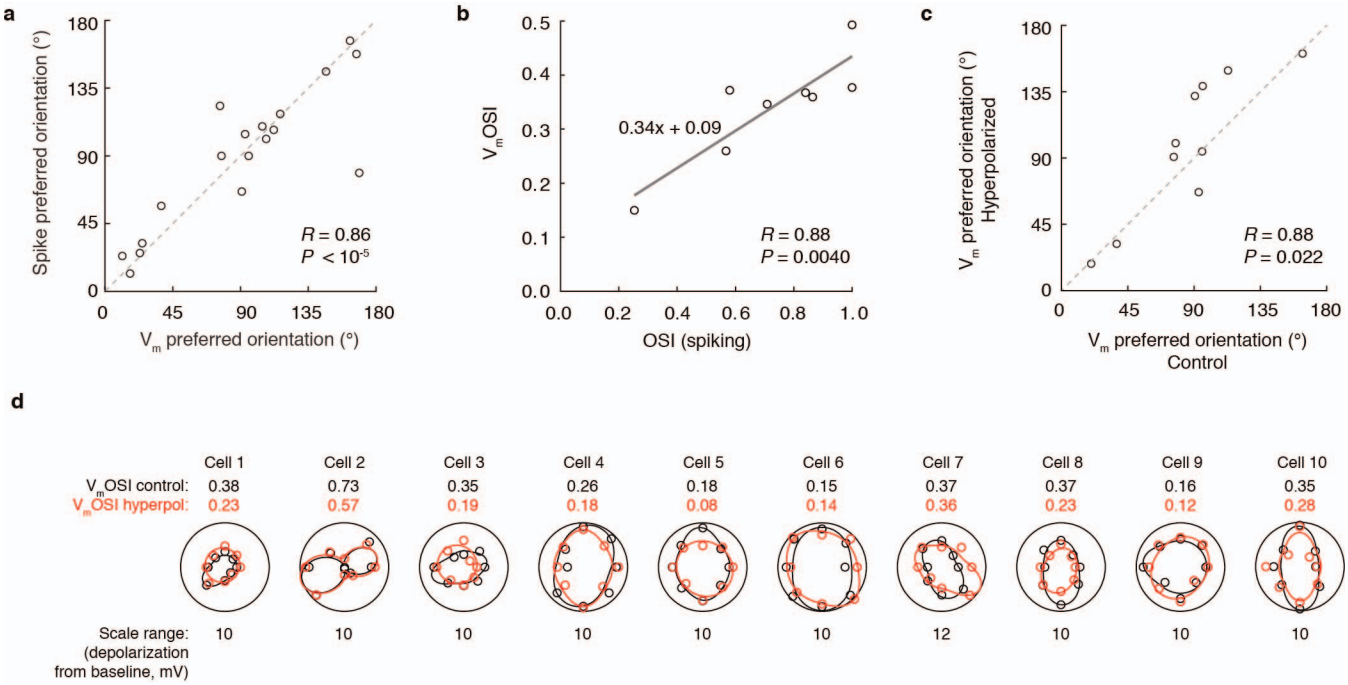

Extended Data Figure 7 | Tuning of action potentials and subthreshold membrane potential. **a**, In individual cells, the orientation tuning of spikes and the membrane potential were highly correlated, indicating that the tuning of the subthreshold responses was not spurious (mean difference in preferred orientation, 14.8 ± 5.3°). **b**, In individual cells, the orientation selectivity index based on the membrane potential response (V_mOSI) was highly correlated with the conventional spiking-based OSI. **c**, In individual cells, the preferred orientation of the control subthreshold response was correlated with the preferred orientation of the subthreshold response during hyperpolarization. **d**, The black curve is the fitted subthreshold orientation tuning curve (the black circles are raw data points), and the red curve is the subthreshold tuning curve during hyperpolarization (the red circles are raw data points). The V_mOSI values for the control and hyperpolarized conditions are shown next to each plot. The radial axes are linear and start at 0. The maximal radial axis range is shown below each polar plot. The differences in V_mOSI are quantified in Fig. 5g.

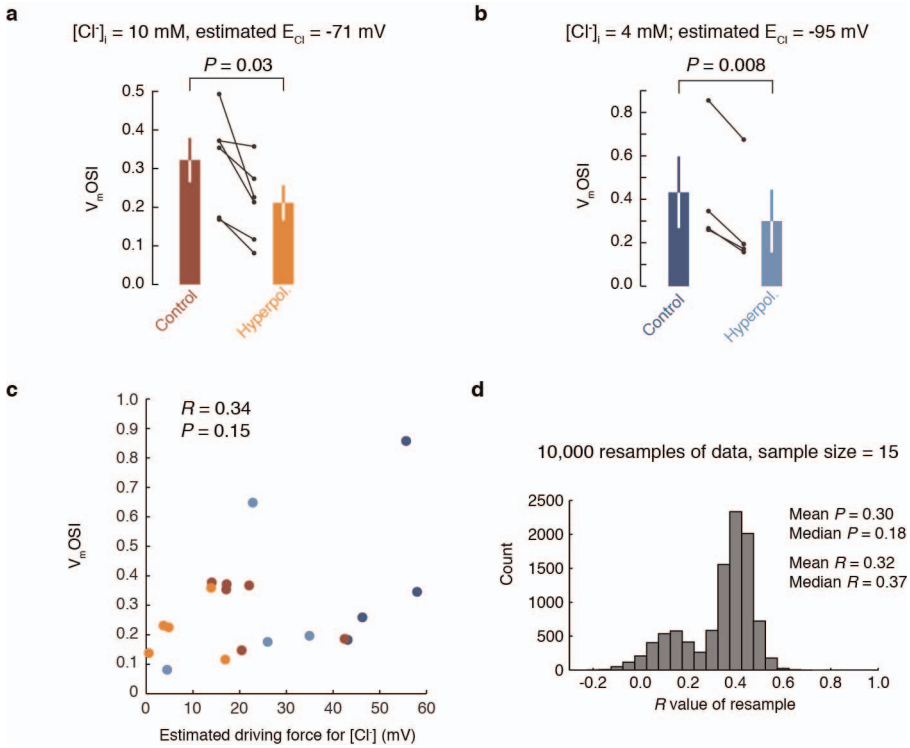

Extended Data Figure 8 | Changes in the driving force for Cl^- do not account for the effects of hyperpolarization on V_mOSI. **a**, When the pipette solution contained 10 mM Cl^-, the reversal potential for chloride, E_{Cl}, was estimated to be −71 mV (based on the assumption that natural cerebrospinal fluid contains a similar amount of Cl^- to the artificial cerebrospinal fluid used). In this situation, hyperpolarization decreased the orientation selectivity index. **b**, Even with a low Cl^- concentration (4 mM; estimated E_{Cl}, −95 mV), the result was the same. **c**, There was no significant correlation between the driving force for Cl^- and V_mOSI. **d**, The data were resampled (15 of the data points in **c** were selected at random, and the *R* and *P* values for that set of data points were calculated; this process was repeated 10,000 times), and this process confirmed that the result from the correlational analysis in **c** was not biased by a small subset of the data points (the mean *R* and *P* values from the resampling analysis match the values for the full data set in **c** well).

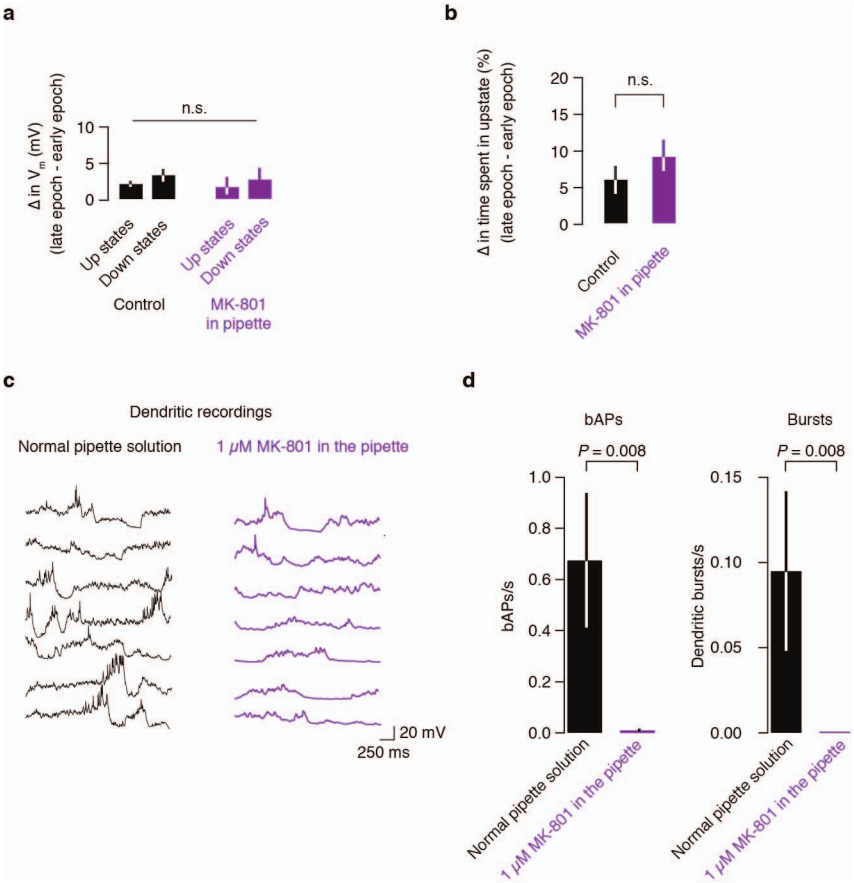

Extended Data Figure 9 | The effect of intracellular MK-801 on up and down states and dendritic spikes. **a**, To determine whether MK-801 that might have leaked out of the pipette during patching affects network circuitry, we examined the dynamics of up and down states in recordings in which MK-801 was in the pipette and in control recordings (no MK-801). **b**, Although, in general, the membrane potential drifted up slightly (<5 mV on average) and the time spent in the up state increased over long recordings (possibly due to the anaesthesia wearing off), these trends were identical with or without MK-801 in the patch pipette. **c**, When 1 μM MK-801 was included in the recording pipette, the visually evoked responses contained fewer bAPs and bursts. This trend was clear in individual cells (**a**) and across the population (**d**). This reduction in spiking confirms that dendritic bursts do not occur when NMDA receptors are blocked. Because the low firing rate in MK-801 recordings prevented a reliable measurement of orientation tuning in the MK-801 dendritic patch-clamp recordings, we averaged over all of the stimulus presentations for both conditions, resulting in a lower average firing rate for bAPs and dendritic bursts.

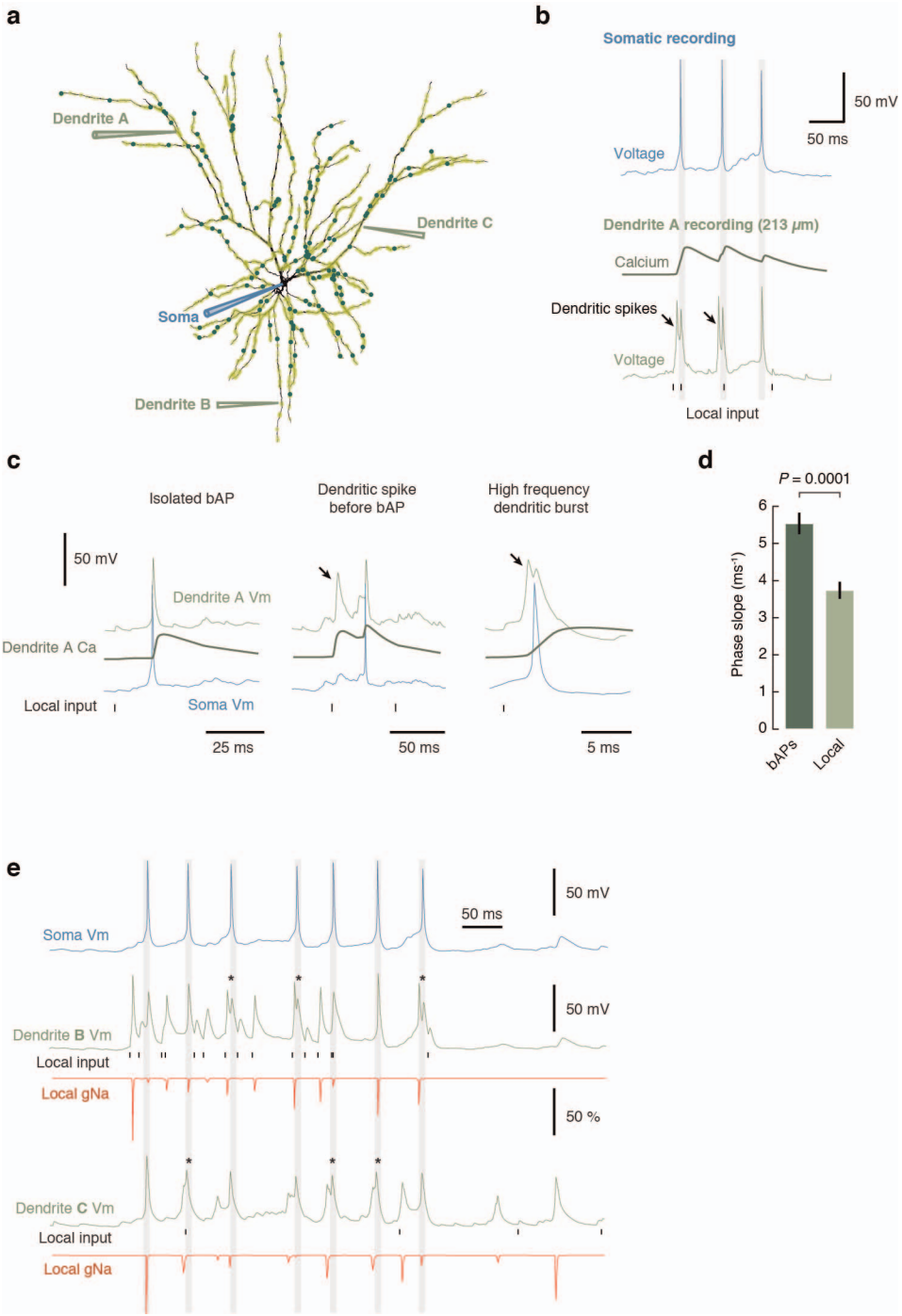

Extended Data Figure 10 | Compartmental modelling of dendritic events. **a**, A detailed reconstruction of a layer 2/3 pyramidal cell was used in the simulations. Light green circles over the dendritic tree represent background synapses, and dark green circles represent signal synapses (the model had 1,100 synapses; not all are illustrated). Voltage was recorded at the soma and at all dendritic branches simultaneously. **b**, Activation of signal synapses at 5 Hz produced high-frequency dendritic bursts, composed of local dendritic spikes and bAPs. These bursts were always accompanied by dendritic Ca^{2+} transients. The timing of the activation of excitatory synapses on the recorded dendritic branch is illustrated. Note how the local excitatory postsynaptic potentials (EPSPs) are clearly smaller than the dendritic spikes. **c**, Examples of specific features consistently observed in the model. Isolated bAPs were associated with global Ca^{2+} transients and had kinked onsets. Dendritic spikes often preceded somatic action potentials, had smooth onsets and Ca^{2+} transients that were localized to the branches where the spikes were recorded, and clearly started before the global transients associated with bAPs. Local dendritic spikes initiated in the dendrite could often be recorded in multiple electrotonically close dendritic branches. Pairs of local spikes and bAPs reached very high frequencies; the example shows a pair at >400 Hz. When NMDA receptors were removed from the simulations, no dendritic spikes were observed, and the soma failed to reach the threshold for action potential firing. This also occurred when there were no dendritic voltage-activated Na^+ channels, indicating that the generation of dendritic spikes is required for producing axonal output. **d**, Quantification of spike onset for local dendritic spikes and bAPs in the model reproduced the experimentally observed effect reported in Extended Data Fig. 5d. **e**, Example trial showing the somatic voltage and recordings for two dendrites indicated in **a**. For each dendrite, the local voltage, the Na^+ channel conductance (gNa, expressed as a fraction of the maximum conductance) and the timing of activation of excitatory synapses on the recorded dendrite are shown. The gNa traces show that there is significant local Na^+ channel inactivation after the first spike and that subsequent spikes are associated with varying degrees of Na^+ channel conductance. Asterisks denote extreme cases when a bAP followed a local dendritic spike at very high frequency and did not recruit any local gNa, thereby indicating that the propagation into the recorded branch was passive.